

Global Tensor Motion Planning

An T. Le¹, Kay Hansel¹, João Carvalho¹, Joe Watson^{1,2}, Julen Urain^{1,5}, Armin Biess, Georgia Chalvatzaki^{1,5} and Jan Peters^{1,2,3,4}

Abstract—Batch planning is increasingly crucial for the scalability of robotics tasks and dataset generation diversity. This paper presents Global Tensor Motion Planning (GTMP)—a sampling-based motion planning algorithm comprising only tensor operations. We introduce a novel discretization structure represented as a random multipartite graph, enabling efficient vectorized sampling, collision checking, and search. We provide an early theoretical investigation showing that GTMP exhibits probabilistic completeness while supporting modern GPU/TPU. Additionally, by incorporating smooth structures into the multipartite graph, GTMP directly plans smooth splines without requiring gradient-based optimization. Experiments on lidar-scanned occupancy maps and the MotionBenchMarker dataset demonstrate GTMP’s computation efficiency in batch planning compared to baselines, underscoring GTMP’s potential as a robust, scalable planner for diverse applications and large-scale robot learning tasks.

I. INTRODUCTION

Motion planning with probabilistic completeness has been a foundation of robotics research, with seminal works like PRM [1] and RRTConnect [2] serving as cornerstone methods for years [3]. However, as the complexity of robotic tasks grows, there is a growing demand for batch-planning methods. Several factors drive this interest: (i) the need to gather large datasets for policy learning [4]–[6], (ii) the inherent non-linearity of task objectives that lead to multiple local minima [7]–[9], and (iii) the increasing availability of powerful GPUs or TPUs for planning [10], [11].

Despite these advancements, batching traditional sampling-based planners, such as RRT/PRM and their variants, remains an ongoing challenge [12]–[15]. Their underlying discretization techniques, such as the incremental graph construction of RRT/PRM or the search mechanism of A* [16], [17], are not conducive to efficient vectorization over planning instances. This paper revisits classical motion planning, introducing a simple yet effective discretization structure with layers of waypoints, which can be represented as tensors, enabling GPU/TPU utilization. We propose Global Tensor Motion Planning (GTMP), which enables highly batchable operations on multiple planning instances, such as batch collision checking and batch Value Iteration (VI) while maintaining an easily vectorizable implementation with JAX [18]. This simplicity allows for differentiable planning and rapid integration with modern frameworks, making the algorithm particularly desirable for real-time applications and scalable data collection for robot learning. Our experimental results demonstrate x300 faster in batch planning than OMPL with PyBullet collision-checking while

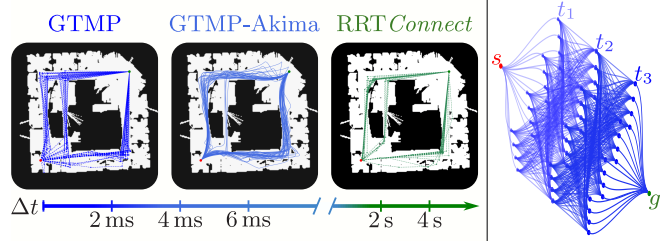


Fig. 1. (Left) Planning comparison of a batch 100 instances on Intel Lab occupancy map. We vectorize planning with GTMP and GTMP-Akima on an RTX3090, filtering-out collided paths, taking a few milliseconds after Just-In-Time compilation (JIT) [18]. OMPL/RRTConnect [19] is run in a loop with a single core of AMD Ryzen 5900X, which takes a few seconds (including simplification time and can be divided by the total number of CPU cores if using CPU parallelization). (Right) Spline discretization graph example of $M = 3$ layers. The spline structure computation can be vectorized over planning instances with the Akima interpolation method [20]. More information can be found on <https://sites.google.com/view/gtmp>

achieving better smoothness and path diversity with *spline discretization structure*.

Our contributions are twofold: i) we propose a *vectorizable sampling-based planner* exhibiting probabilistic completeness, which does not require simplification routines [19], and ii) we extend GTMP with a *spline discretization structure*, enabling batch C^1 spline planning with path quality comparable to trajectory optimizers.

II. RELATED WORKS

Vectorizing motion planning has been an active research topic for decades. Here, we briefly survey the most relevant works on vectorizing either at the *algorithmic-level* (e.g., collision-checking) or *instance-level* (e.g., batch trajectory planning).

Sampling-based Vectorization. Recognizing the importance of planning parallelization, earliest works [12], [13], [15], [21], [22] propose a *vectorizable* collision-checking data structure. State-of-the-art work on leveraging CPU-based *single instruction, multiple data* [23] (i.e., VAMP) has pushed collision-checking efficiency to *microseconds*. In a different vein, a body of works [24]–[29] proposes a learning heuristic or batch-sampling strategies to inform or refine the search-graph with new samples, effectively reducing collision checkings. Despite the hardware or algorithmic acceleration efforts, past works still resort to discretization structures such as trees (for RRT variants) or graphs (for PRM variants) [30], which are unsuitable for instance-level vectorization.

Vectorizing Trajectory Optimization. Vectorizing optimization-based planner with GPU-acceleration [7], [10], [11], [31]–[33] gained traction recently due to their computational efficiency, the solutions’ multi-modality and

¹Intelligent Autonomous Systems Lab, TU Darmstadt, Germany; ²German Research Center for AI (DFKI); ³Hessian.AI; ⁴Centre for Cognitive Science. ⁵Interactive Robot Perception & Learning Lab, TU Darmstadt, Germany; Corresponding author: An T. Le, an@robot-learning.de

their robustness to bad local-minima. However, these local methods are sensitive to initial conditions and may get stuck in large infeasible regions. GTMP addresses this issue by proposing a layerwise discretization structure, enabling vectorization in sampling and search operations while having better global solutions.

III. PROBLEM DEFINITION

We consider the path planning problem [34] in a compact configuration space $\mathcal{C} \subset \mathbb{R}^d$ having d -dimensions, with $\mathcal{C}_{\text{coll}}$ being the collision space such that $\mathcal{C} \setminus \mathcal{C}_{\text{coll}}$ is open. Let $\mathcal{C}_{\text{free}} = \text{cl}(\mathcal{C} \setminus \mathcal{C}_{\text{coll}})$ be the free space, with $\text{cl}(\cdot)$ the set closure. Denote the start configuration \mathbf{q}_0 and a set of goal configurations \mathcal{G} . The path planning problem is defined by the triplet $(\mathcal{C}_{\text{free}}, \mathbf{q}_0, \mathcal{G})$. Let $f : [0, 1] \rightarrow \mathbf{q}$, we can define its total variation as its arc length

$$\text{TV}(f) = \sup_{M \in \mathbb{N}, 0=t_0, \dots, t_M=1} \sum_{i=1}^M \|f(t_i) - f(t_{i-1})\| \quad (1)$$

Definition 1 (Feasible Path). *The function $f : [0, 1] \rightarrow \mathbf{q}$ with $\text{TV}(f) < \infty$ is*

- a path, if it is continuous.
- a feasible path, if and only if $\forall t \in [0, 1], f(t) \in \mathcal{C}_{\text{free}}, f(0) = \mathbf{q}_0, f(1) \in \mathcal{G}$.

Let \mathcal{F} be the set of all paths.

Problem 1 (Feasible Path Planning). *Given a planning problem $(\mathcal{C}_{\text{free}}, \mathbf{q}_0, \mathcal{G})$ and cost function $c : \mathcal{F} \rightarrow \mathbb{R}_{>0}$, find a feasible path f and report failure if no feasible path exists.*

Here, we do not consider dynamics constraints, invalid configurations that violate collision constraints and configuration limits. This problem definition is standard for several robotic settings, such as serial manipulators with joint limits.

IV. TENSORIZING MOTION PLANNING

GTMP leverages a fixed discretization structure, represented as a random multipartite graph, to enable efficient planning vectorization. This approach contrasts with the incremental discretization structures of classical motion planning algorithms, which procedurally expand the search space during planning.

A. Discretization Structure

We introduce the random multipartite graph as a novel configuration discretization structure designed for seamless representation using tensors.

Definition 2 (Random Multipartite Graph Discretization). *Consider a geometric graph $G = (\mathcal{V}, \mathcal{E})$ on configuration space \mathcal{C} , the node set \mathcal{V} is represented by $\{\mathbf{q}_s, \mathcal{M}, \mathcal{G}\}$, where $\mathcal{M} = \{\mathcal{L}_m\}_{m=1}^M$ is a set of M layers. Each layer $\mathcal{L}_m = \{\mathbf{q}_i \in \mathcal{C} \mid \mathbf{q}_i \sim p_m\}_{i=1}^N$ contains N waypoints sampled by an associated proposal distribution p_m on \mathcal{C} . The edge set \mathcal{E} is defined by the union of (forward) pair-wise connections between the start and first layer $\{(\mathbf{q}_s, \mathbf{q}) \mid \forall \mathbf{q} \in \mathcal{L}_1\}$, between layers in \mathcal{M}*

$$\{(\mathbf{q}_m, \mathbf{q}_{m+1}) \mid \forall \mathbf{q}_m \in \mathcal{L}_m, \mathbf{q}_{m+1} \in \mathcal{L}_{t+1}, 1 \leq m < M\},$$

and between the last layer and goals $\{(\mathbf{q}, \mathbf{q}_g) \mid \forall \mathbf{q} \in \mathcal{L}_M, \mathbf{q}_g \in \mathcal{G}\}$, leading to a complete $(M+2)$ -partite directed graph.

We typically set $p_m = \mathcal{U}(\mathcal{C})$ as uniform distributions over configuration space (bounded by configuration limits cf. Fig. 2). Extending Definition 2 to *spline discretization structure* by replacing the straight line with the cubic polynomials, representing any edge $(\mathbf{q}, \mathbf{q}') \in \mathcal{E}$, is straightforward with Akima spline [20], [35] (cf. Appendix).

Definition 3 (Path In G). *A path $f : [0, 1] \rightarrow \mathbf{q}$ in G exists if it $f(0) = \mathbf{q}_0, f(1) \in \mathcal{G}$ and its piecewise linear segments correspond to edges connecting \mathbf{q}_0 and $\mathbf{q}_g \in \mathcal{G}$.*

B. Deterministic Markov Decision Process On Graph

We augment a Deterministic Markov Decision Process (DMDP) on G by the tuple $(\mathcal{V}, \mathcal{E}, c, t, \gamma)$, where the state set is the node set of G , the action set is equivalent to the edge set \mathcal{E} , the transition cost function $c : \mathcal{V} \times \mathcal{E} \rightarrow \mathbb{R}$, deterministic state transition probability $t(\mathbf{q}' \mid \mathbf{q}, (\mathbf{q}, \mathbf{q}')) = 1, (\mathbf{q}, \mathbf{q}') \in \mathcal{E}$ and discount factor $\gamma \in [0, 1)$. The goal set $\mathcal{G} \subset \mathcal{V}$ is the terminal set with terminal costs $c_g(\mathbf{q}), \mathbf{q} \in \mathcal{G}$. A policy $\pi : \mathcal{V} \rightarrow \mathcal{E}$ depicts the decision to transition to the next layer given the current state at the current layer.

We employ typically unbounded occupancy collision cost

$$c_{\text{coll}}(\mathbf{q}) = 0 \text{ if } \mathbf{q} \in \text{int}_\delta(\mathcal{C}_{\text{free}}), \text{ else } \infty, \quad (2)$$

which merges the planning and verification steps (cf. Theorem 1). Then, the transition cost function can be defined

$$c(\mathbf{q}, (\mathbf{q}, \mathbf{q}')) = \underbrace{\int_a^b (c_{\text{coll}}(\mathbf{q}(t))) \alpha dt}_{\text{collision}} + \underbrace{\|\mathbf{q} - \mathbf{q}'\|}_{\text{smoothness}}, \quad (3)$$

where the collision term is a straight-line integral with $\alpha = 1/\|\mathbf{q}' - \mathbf{q}\|$ between $\mathbf{q}(a) = \mathbf{q}$ and $\mathbf{q}(b) = \mathbf{q}'$. Finding the optimal value function for this DMDP is straightforward with the Bellman optimality operator

$$\begin{aligned} v_G(\mathbf{q}) &\leftarrow \min_{(\mathbf{q}, \mathbf{q}')} \sum_{\mathbf{q}'} t(\mathbf{q}' \mid \mathbf{q}, (\mathbf{q}, \mathbf{q}')) (c(\mathbf{q}, (\mathbf{q}, \mathbf{q}')) + \gamma v_G(\mathbf{q}')) \\ &\leftarrow \min_{(\mathbf{q}, \mathbf{q}')} (c(\mathbf{q}, (\mathbf{q}, \mathbf{q}')) + \gamma v_G(\mathbf{q}')) \end{aligned} \quad (4)$$

It is well-known that Eq. (4) converges to a fixed point [36], and the optimal policy is extracted by tracing the optimal value function

$$\pi^*(\mathbf{q}) = \underset{(\mathbf{q}, \mathbf{q}')}{\text{argmin}} (c(\mathbf{q}, (\mathbf{q}, \mathbf{q}')) + \gamma v_G^*(\mathbf{q}')), \quad (5)$$

from \mathbf{q}_0 until $\mathbf{q}' \in \mathcal{G}$. This produces a sequence of edges $\mathcal{P} = \{(\mathbf{q}_0, \mathbf{q}_1), \dots, (\mathbf{q}_M, \mathbf{q}_g) \mid \mathbf{q}_g \in \mathcal{G}\}$.

Proposition 1. *By following any policy on $(\mathcal{V}, \mathcal{E}, c, t, \gamma)$ from \mathbf{q}_0 , \mathcal{P} has a constant cardinality of $M + 1$.*

Proof. By construction of graph G , each application of Eq. (5) increases the layer number m strictly monotonically, since $t(\mathbf{q}_{m+1} \mid \mathbf{q}_m, \pi(\mathbf{q}_m)) = t(\mathbf{q}_{m+1} \mid \mathbf{q}_m, (\mathbf{q}_m, \mathbf{q}_{m+1})) = 1, (\mathbf{q}_m, \mathbf{q}_{m+1}) \in \mathcal{E}$. Hence, $|\mathcal{P}| = M + 1$. \square

Finding optimal paths by VI over a discretization structure has been a common practice and widely applied in different settings [37]. We are the first to apply VI over a multipartite graph, enabling batching mechanisms over planning instances, as we present in the next section.

C. Batching The Planner

In practice, we do not need to construct an explicit graph data structure due to G 's multipartite structure. Observing the deterministic state transition and the equal cardinality of layers, we just need to compute and maintain the transition cost matrices $\mathbf{C}_s \in \mathbb{R}^M$, $\mathbf{C}_h \in \mathbb{R}^{(M-1) \times N \times N}$, $\mathbf{C}_l^{N \times |\mathcal{G}|}$ and value matrices $\mathbf{V}_s \in \mathbb{R}$, $\mathbf{V}_h \in \mathbb{R}^{M \times N}$, $\mathbf{V}_g \in \mathbb{R}^{|\mathcal{G}|}$, where \mathbf{C}_s is the transition costs from \mathbf{q}_0 to the first layer; $\mathbf{C}_h, \mathbf{C}_l$ hold transition costs between middle layers and last layer to goals; $\mathbf{V}_s, \mathbf{V}_h, \mathbf{V}_g = \mathbf{C}_g$ hold values of start, layers costs and terminal goal costs. First, we sample in batches the waypoints for all layers $\mathbf{Q} \in \mathbb{R}^{M \times N \times d}$ within the state limits and form the goal configuration $\mathbf{G} \in \mathbb{R}^{|\mathcal{G}| \times d}$ from \mathcal{G} . The cost-to-go term of the transition costs Eq. (3) is approximately computed by first probing an H number of equidistant points on all edges, evaluating them in batches, and taking the mean values over the probing dimension. We assume all cost functions are batch-wise computable. Then, the Bellman optimality operator Eq. (4) becomes

$$\begin{aligned} \mathbf{V}_h[M-1] &\leftarrow \min(\mathbf{C}_l + \gamma \mathbf{V}_g) \\ \mathbf{V}_h[:M-1] &\leftarrow \min(\mathbf{C}_h + \gamma \mathbf{V}_h[1:], \text{axis} = -1) \quad (6) \\ \mathbf{V}_s &\leftarrow \min(\mathbf{C}_s + \gamma \mathbf{V}_h[0]) \end{aligned}$$

Given the converged value matrix \mathbf{V}_h^* , a sequence of indices is traced by Eq. (5) (cf. Algorithm 1), which is used to extract the waypoints from \mathbf{Q} and \mathbf{G} . Notice that all component matrices can be straightforwardly vectorized by adding the batch dimension B for all matrices. Note that [12]–[14], [23] focus on vectorizing collision checking or forward kinematics in a single planning instance, while we can ensure that Eqs. (4) and (5) can be vectorized at instance-level [7] by Proposition 1.

Complexity Analysis. Eq. (6) is an asynchronous update in batches (i.e., updates based on values of previous iteration) and also known to converge [38]. Considering the layer number M , waypoint number per layer N , and probing number H , we assume that Eq. (6) is executed on P processor units, a rough estimate of time complexity per VI iteration is $\mathcal{O}(MN/P)$, since the layers are independently updated and each processing unit is assigned M/P layers. [39] shows that the worst-case complexity of VI for any MDP is $K = \mathcal{O}(1/(1-\gamma) \log(1/(1-\gamma)))$, where K is the convergence rate of Bellman optimality operator. Hence, the

Algorithm 1: Tracing the optimal path from \mathbf{V}^*

```

1  $i \leftarrow \operatorname{argmin}(\mathbf{C}_s + \gamma \mathbf{V}_h^*[0])$ 
2  $\mathcal{P} = \{i\}$ 
3 for  $1 \leq m \leq M-1$  do
4    $i \leftarrow \operatorname{argmin}(\mathbf{C}_h[i-1] + \gamma \mathbf{V}_h^*[i])$ 
5   Append  $i$  to  $\mathcal{P}$ 
6 Append  $\operatorname{argmin}(\mathbf{C}_l[i] + \gamma \mathbf{V}_g^*)$  to  $\mathcal{P}$ 
Output:  $\mathcal{P}$ 

```

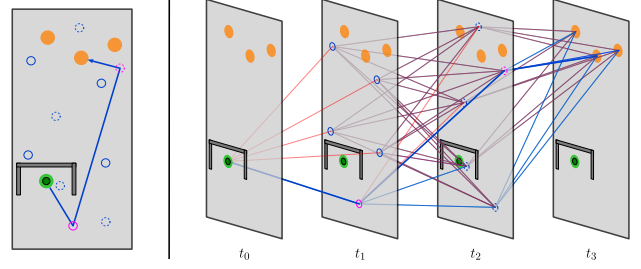


Fig. 2. Example diagram of GTMP. The objective is to find a feasible path from the start (green) and the goals (yellow). Each layer uniformly samples 5 waypoints.

overall worst-case time complexity is $\mathcal{O}(KMN/P)$. The collision-checking time complexity is $\mathcal{O}(MN^2H/P)$, and thus, the overall time complexity is $\mathcal{O}(MN(NH+K)/P)$. The space complexity is $\mathcal{O}(MN^2H)$ due to the collision check values.

V. THEORETICAL ANALYSIS

Notations. We denote \mathcal{F} as the set of feasible paths for a feasible planning problem. Let \mathcal{R} be the set of all paths in G . The path cost is the sum of (discounted) straight-line integrals over the edges $c(g) = \sum_{m=0}^M \gamma^m c(\mathbf{q}_m, \mathbf{q}_{m+1}) + c_g(g(1))$, $g \in \mathcal{R}$.

Assumption 1. We assume that all associated proposal distributions at each layer are uniformly distributed on the configuration space $\forall 1 \leq m \leq M$, $p_m := \mathcal{U}(\mathcal{C})$.

Assumption 2. Consider a feasible planning problem, there exists a feasible path $f : [0, 1] \rightarrow \mathcal{C}_{\text{free}}$ having margin $r = \inf_{t \in [0, 1]} \|f(t) - \mathbf{q}\|$, $\mathbf{q} \in \mathcal{C}_{\text{coll}}$, such that $r > 0$.

This assumption is common in path planning applications, where the free-path set is not zero-measure $\mu(\mathcal{F}) \neq 0$.

Theorem 1 (Feasibility Check). For any planning problem with $\gamma > 0$, $v_G^*(\mathbf{q}_0) < \infty$ if and only if there exists a feasible path in G .

Proof. According to Bellman optimality, $v_G^*(\mathbf{q}_0) = \min_g \{c(g) \mid g \in \mathcal{R}\}$ is the minimum path cost reaching the goals. By definition, the smoothness term in Eq. (3) is bounded with $\forall \mathbf{q} \in \mathcal{C}$, since $\text{TV}(g) < \infty$. Thus, with $\gamma > 0$, any unbounded path cost $c(\mathcal{P}) = \infty$ occurs, if and only if $\exists t, f(t) \in \mathcal{C}_{\text{coll}}$. Hence, with $\gamma > 0$, $v_G^*(\mathbf{q}_0) = \min_{\mathcal{P}} \{c(\mathcal{P}) \mid \mathcal{P} \in \mathcal{R}\} < \infty$, if and only if $\exists \mathcal{P} \in \mathcal{R}$, $c(\mathcal{P}) < \infty$. \square

Theorem 1 is useful to filter collided paths after VI.

Lemma 1 (Solvability In Finite Path Segments). If assumption 2 holds, there exists a minimum number of segments $M_m \in \mathbb{N}_{>0}$ for piecewise linear paths to be feasible.

Proof. We first show that there exists a piecewise linear path $g : [0, 1] \rightarrow \mathcal{C}$ such that $\|f - g\|_\infty < r$, where $\|f - g\|_\infty = \max_{t \in [0, 1]} \|f(t) - g(t)\|$. We construct g by dividing the interval $[0, 1]$ into M subintervals with length less than $\delta > 0$, i.e., $[t_0, t_1], \dots, [t_{M-1}, t_M]$ with $0 = t_0 < t_1 < \dots < t_M = 1$. On each subinterval $[t_m, t_{m+1}]$, we

define the corresponding segment of g to approximate f

$$g(t) = f(t_m) + \frac{f(t_{m+1}) - f(t_m)}{t_{m+1} - t_m}(t - t_m), t \in [t_m, t_{m+1}]. \quad (7)$$

Since by definition the path f is continuous on a compact interval $[0, 1]$, then by Heine-Cantor theorem, f is also uniformly continuous, i.e., $\exists \delta > 0$ for any $a, b \in [0, 1]$, $|a - b| < \delta$, then $\|f(a) - f(b)\|_\infty < r$. Then, by the construction of g and uniform continuity of f , we can choose a δ sufficiently small such that $\|f - g\|_\infty < r$. This implies that there exists a sufficiently large number of segments M_m such that δ is sufficiently small, hence, g is a feasible path. \square

Lemma 1 implies that any path planning algorithm producing a piecewise linear feasible path, then it must have a minimum number of segments.

Lemma 2. *Let piecewise linear path $g : [0, 1] \rightarrow \mathcal{C}$ having n equal subintervals approximating a path $f : [0, 1] \rightarrow \mathcal{C}$. The error bound is $\|f - g\|_\infty < L/n$, where $L = TV(f)$ is the total variation of f .*

Proof. Denoting the subinterval length $h = 1/n$ and reusing the notations from Lemma 1 proof, we define g as a piecewise linear function 7. Since f, g are uniformly continuous, the linear interpolation error can be expressed using the modulus of continuity on a segment $t \in [t_m, t_{m+1}]$

$$\|f(t) - g(t)\| < \omega_f(h), \omega_f(h) = \sup_{|a-b| \leq h} \|f(a) - f(b)\|.$$

And, the global error over all segments is

$$\|f(t) - g(t)\|_\infty = \max_{0 \leq m \leq n-1} \sup_{x \in [t_m, t_{m+1}]} \|f(t) - g(t)\|$$

By definition, f is uniformly continuous and of bounded variation, the modulus of continuity $\omega_f(h)$ provides an upper bound for the error on each segment. Therefore, $\|f(t) - g(t)\|_\infty < \omega_f(1/n)$ on $[0, 1]$. For functions of bounded variation, the modulus of continuity can be bounded in terms of the total variation $\omega_f(1/n) < L/n$ on $[0, 1]$. Hence, $\|f(t) - g(t)\|_\infty < L/n$. \square

Lemma 3. *Let g_1, g_2 be a piecewise linear function having the same number of partition points $\{g_1(t_m)\}_{m=0}^M, \{g_2(t_m)\}_{m=0}^M$ with $0 = t_0 < \dots, t_M = 1$, $\|g_1 - g_2\|_\infty < \delta$, if and only if $\|g_1(t_m) - g_2(t_m)\| < \delta$, $0 \leq m \leq M$.*

Proof. Sufficiency. Given $\|g_1(t_m) - g_2(t_m)\| < \delta, \forall 1 \leq m \leq M$, since g_1, g_2 are piecewise linear functions, the linear interpolation between partition points t_m, t_{m+1} ensures that the difference between g_1, g_2 is maximized at the partition points. Consider g_1, g_2 on a segment $[t_m, t_{m+1}]$

$$\|g_1(t) - g_2(t)\| \leq \max\{\|g_1(t_m) - g_2(t_m)\|, \|g_1(t_{m+1}) - g_2(t_{m+1})\|\} < \delta \quad (8)$$

Hence, $\|g_1 - g_2\|_\infty = \max_{t \in [0, 1]} \|g_1(t) - g_2(t)\| < \delta$.

Necessity. Given $\|g_1 - g_2\|_\infty < \delta$, then $\|g_1(t_m) - g_2(t_m)\| < \delta, 0 \leq m \leq M$. \square

Theorem 2 (Probabilistic Completeness). *If assumption 1 and assumption 2 hold, for a feasible planning problem $(\mathcal{C}_{free}, \mathbf{q}_0, \mathcal{G})$, with G having $M \geq M_m$ layers, there exist constants $a, R, L > 0$ depending only on \mathcal{C}_{free} and \mathcal{G} , such that*

$$\mathbb{P}(v_G^*(\mathbf{q}_0) < \infty) > 1 - M \exp\left(-a \left(R - \frac{L}{M+1}\right)^d N\right). \quad (9)$$

Proof. From Lemma 1, if $M \geq M_m$, there exists a feasible piecewise linear path g having $M+1$ segments with $0 = t_0 < \dots < t_{M+1} = 1$ approximating a feasible path f . Let $R = \inf_{t \in [0, 1]} \|f(t) - \mathbf{q}\|, \mathbf{q} \in \mathcal{C}_{coll}, r = \inf_{t \in [0, 1]} \|g(t) - \mathbf{q}\|, \mathbf{q} \in \mathcal{C}_{coll}$ be collision margins of f, g , $\mathcal{B}_\delta(\mathbf{q}) = \{\|\mathbf{q}' - \mathbf{q}\| < \delta, \delta > 0\}$ is an open δ -ball around \mathbf{q} . Now, let's g has equal subinterval.

First, we compute the probability of the event that a sampled graph G has at least a piecewise linear path h with $M+1$ segments such that h is approximating g . h is feasible when $\|h - g\|_\infty < r$. We have

$$\begin{aligned} r &= \inf_{t \in [0, 1]} \|g(t) - \mathbf{q}\|, \mathbf{q} \in \mathcal{C}_{coll} \\ &\leq \inf_{t \in [0, 1]} \|f(t) - \mathbf{q}\|, \mathbf{q} \in \mathcal{C}_{coll} + \inf_{t \in [0, 1]} \|g(t) - f(t)\| \\ &= \inf_{t \in [0, 1]} \|f(t) - \mathbf{q}\|, \mathbf{q} \in \mathcal{C}_{coll} - \sup_{t \in [0, 1]} \|g(t) - f(t)\| \\ &< R - \frac{L}{M+1}, \end{aligned}$$

where the first inequality due to $\mathcal{C} \subset \mathbb{R}^d$, and last inequality from Lemma 2 and $L = TV(f)$.

From Lemma 3, since by definition h, g has the same number of segments, the event $\|h - g\|_\infty < r < r_h = R - \frac{L}{M+1}$ is the event that, given start and goals fixed, for each layer $1 \leq m \leq M$, there is at least one point $h(t_m)$ is sampled inside the ball $\mathcal{B}_{r_h}(g(t_m))$. Then, by sampling N points uniformly over \mathcal{C} per layer (Assumption 1), and the fact that there are pairwise connections between layers, we have the failing probability

$$\begin{aligned} \mathbb{P}(\|h - g\|_\infty \geq r_h) &\leq \sum_{m=1}^M \left(1 - \frac{\mu(\mathcal{B}_{r_h}(g(t_m)))}{\mu(\mathcal{C})}\right)^N \\ &\leq M \exp\left(-\frac{\alpha_d}{\mu(\mathcal{C})} \left(R - \frac{L}{M+1}\right)^d N\right) \end{aligned}$$

where we use the inequality $1 - x \leq e^{-x}, x \geq 0$, and $a = \alpha_d/\mu(\mathcal{C})$, where α_d is the constant term computing volume of a d -ball.

The event of h approximating g having equal intervals is a subset of the event of h approximating g having arbitrary intervals. The event that at least a path h in G having $\|h - g\|_\infty < r_h$ is a subset of the event $\exists a$ feasible path in G , since there might exist multiple feasible paths and their corresponding piecewise linear approximations have $M+1$ segments. From Theorem 1, $v_G^*(\mathbf{q}_0) <$

∞ is equivalent to \exists a feasible path in G . We have

$$\begin{aligned} \mathbb{P}(v_G^*(\mathbf{q}_0) < \infty) &\geq \mathbb{P}(\|h - g\|_\infty < r_h) \\ &> 1 - M \exp\left(-a \left(R - \frac{L}{M+1}\right)^d N\right). \end{aligned}$$

□

The lower bound is intuitive since it directly implies a minimum number of layers $M > \lfloor L/R \rfloor - 1$ (cf. Lemma 1) for the exponent coefficient to be strictly positive. It also implies the existence of an optimal number M^* ; increasing M helps then harms N sample efficiency, depending on the planning problem (cf. Fig. 4).

VI. EXPERIMENT RESULTS

We assess the performance of GTMP and its extension w.r.t. task success, success path diversity, and smoothness compared to popular baselines and collision-checking mechanisms. Hence, we investigate the following questions for batch trajectory generation, or for finding the global solution: i) how does GTMP with JAX/GPU-implementation compare to highly optimized probabilistic-complete planners implemented in PyBullet/OMPL [19], [40] or in VAMP [23]?, ii) how does GTMP-Akima compare to popular gradient-based smooth trajectory optimizers such as CHOMP [41] or GPMP [8]?, and iii) Can the probabilistic completeness Theorem 2 be verified experimentally?

We run all CPU-based planners (RRTC, BKPIECE) on AMD Ryzen 5900X clocked at 3.7GHz and GPU-based planners (GTMP, CHOMP, and GPMP) on a single Nvidia RTX 3090. Note that all GPU-based planners are implemented in JAX [18], and the planning times are measured after JIT¹. We set a default probing $H = 10$ and use uniform sampling for all GTMP runs. For all CPU-based planners, we give a timeout of one minute and report metrics after simplification routines. Planning time per task is the sum of all planning instances, which includes simplification time for CPU-based planners, while GTMP does not need path simplification.

Metrics. The metrics are chosen for comparing across probabilistically-complete planners and trajectory optimizers: (i) *Planning Time* (s) in seconds of a batch of paths given a task, (ii) *Collision Free* (CF %) percentage of paths in a batch (failure cases are either in collision or timeout), (iii) *Minimum/Mean Cosine Similarities* (*Min Cosim*/*Mean Cosim*) over consecutively path segments and averaging over the batch of paths in a task, (iv) *Paths Diversity* (PD) as the mean of pairwise Sinkhorn [42] distances in a batch having B paths

$$PD = \frac{1}{B(B-1)} \text{OT}_\lambda(\mathcal{P}_i, \mathcal{P}_j), i, j \in \{1, \dots, B\}, \quad (10)$$

where we treat the path $\mathcal{P} = \{\mathbf{q}_0, \dots, \mathbf{q}_T\}$ as empirical distribution with uniform weights, and different paths can have different horizons T . The entropic scalar $\lambda = 5e^{-3}$ is constant. The metric *Min/Mean Cosim* measures the worst/average rough turns over path segments, while the

¹Planning functions are JITed before all experiments.

PD measures the spread of solution paths correlating to solutions' modes discovery.

A. Planar Occupancy Dataset

Fig. 3 (top-row) compares GTMP ($M=200$, $N=4$) with OMPL implementation of (single-query) RRTConnect [2] and BKPIECE [43]. The environments are planar occupancy maps of Intel Lab, ACES3 Austin, Orebro, Freiburg Campus, and Seattle UW Campus generated from the Radish dataset [44]. The maps are chosen to include narrow passages, large spaces, and noisy occupancies (cf. Fig. 1). We randomly sample 100 start-goal pairs as tasks on each map and plan 100 paths per task.

We clearly see a comparable Min/Mean Cosim (i.e., similar statistics of rough turns) and PD of GTMP ($M=200$, $N=4$) compared to baselines across maps and in aggregated statistics over maps (cf. Table I). With JIT and GPU utilization, GTMP consistently produces batch paths with a fixed number of segments and x250 less wall-clock time compared to baselines across maps.

B. Motion Bench Maker Dataset

We choose the standard MOTIONBENCHMARKER (MBM) dataset [45] of challenging 7-DoF Franka Emika Panda tasks such as table-top manipulation (*table pick and table under pick*), reaching (*bookshelf small, tall and thin*), and highly-constrained reaching (*box and cage*). Each task is pre-generated with 100 problems available publicly. We implement our collision-checking in JAX via primitive shape approximation, such as a Panda spherized model, oriented cubes, and cylinders representing tasks in MBM. The default hyperparameters and compilation configurations for VAMP/RRTC, OMPL/RRTC, and OMPL/BKPIECE are also adopted following [23]². CHOMP and GPMP plan first-order trajectories having an horizon of $T = 32$. All algorithms are compared on the planning performance of a batch of $B = 50$ paths for all tasks.

Fig. 3 (bottom-row) shows the planning performance comparisons between GTMP ($N=30$, $M=2$) and baseline probabilistically-complete planners and gradient-based trajectory optimizers. We see that GTMP consistently has the best diversity (PD) and worst rough turn statistics (Min Cosim) in all tasks. This is due to the maximum exploration behavior of GTMP by sampling uniformly over configuration space, which increases the risk of rough paths. In principle, increasing points per layer N while having minimum solving layers M would improve Min Cosim due to having more chances to discover smoother paths with fewer segments, as long as GPU memory allows (cf. Fig. 4). Compared with gradient-based optimizers on Table II, GTMP-Akima

²We use default *shortcut* simplification for OMPL planners while using default *shortcut and B-spline smoothing* for VAMP/RRTC.

TABLE I
AGGREGATED STATISTICS OF OCCUPANCY EXPERIMENT

Algorithms	PT ↓ (ms)	CF ↑ (%)	Mean Cosim ↑	Min Cosim ↑	PD ↑
GTMP (N=200, M=4)	9.9 ± 1.5	62.2 ± 29.7	0.48 ± 0.19	-0.06 ± 0.32	11.0 ± 9.4
RRTC	2705.9 ± 0.9	84.0 ± 36.6	0.71 ± 0.11	0.13 ± 0.57	10.8 ± 9.4
BKPIECE	3529.9 ± 0.5	84.0 ± 36.6	0.67 ± 0.13	0.07 ± 0.54	13.1 ± 9.9

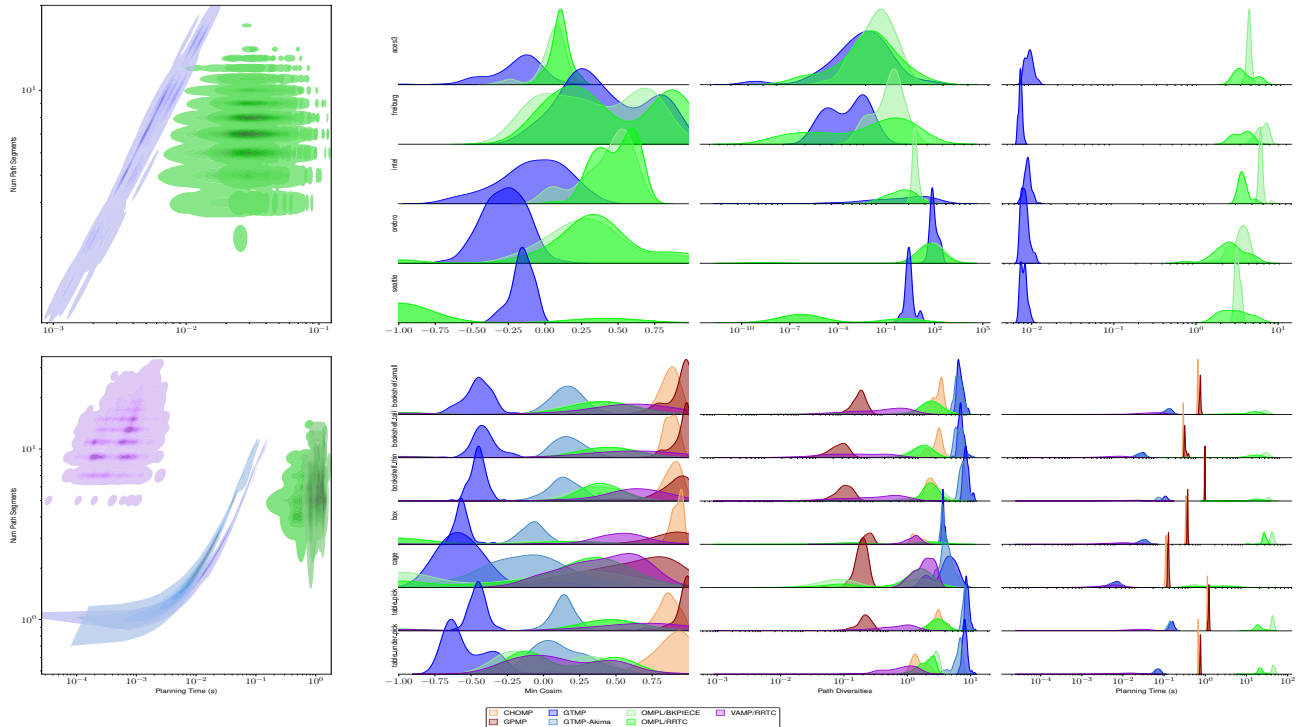


Fig. 3. Comparison experiment on Planar Occupancy and Panda MBM dataset. We note the log scale on PD and Planning Time plots. All plotted data points are based on successful path statistics. Missing distributions of baselines are due to zero success rate on a task.

with spline discretization construction has a similar Mean Cosim to CHOMP and GMP while not requiring gradients from the planning costs. However, GTMP-Akima still suffers from worst-case rough turns due to limited N by memory constraints. On batch planning efficiency, GTMP and GTMP-Akima achieve same order of magnitude planning time with state-of-the-art VAMP/RRTC implementation while being x10 faster than CHOMP/GMP and x300 faster than the OMPL implementation with PyBullet collision checking. We leave the investigation of combining GTMP with the VAMP collision checking for future work, when the VAMP batch configuration collision checking feature becomes available.

Fig 3 (first-column) shows the distributions of planning time versus number of path segments, reflecting inherent algorithmic differences between GTMP and RRTC implementations. RRTC blobs are spread due to differences in randomized graph explorations between planning instances and are separated due to differences in collision-checking efficiency [23]. GTMP batches planning via layered structure, resulting in predictable narrow distribution due to fixed-segment path planning.

TABLE II
AGGREGATED STATISTICS OF PANDA MBM EXPERIMENT

Algorithms	PT ↓ (ms)	CF ↑ (%)	Mean Cosim ↑	Min Cosim ↑	PD ↑
GTMP (N=30, M=2)	55.9 ± 18.6	71.1 ± 37.4	-0.27 ± 0.11	-0.48 ± 0.11	7.1 ± 1.3
GTMP-Akima (N=30, M=2)	48.8 ± 13.1	48.0 ± 38.9	0.92 ± 0.01	0.08 ± 0.18	6.4 ± 1.9
OMPL/RRTC	1.8 ± 0.9e ⁴	68.3 ± 46.5	0.43 ± 0.24	0.13 ± 0.53	1.3 ± 0.9
OMPL/BKPIECE	3.5 ± 1.5e ⁴	65.8 ± 47.4	0.39 ± 0.25	0.04 ± 0.56	1.3 ± 1.1
VAMP/RRTC	10.6 ± 12.5	100.0 ± 0.0	0.82 ± 0.2	0.43 ± 0.43	0.65 ± 0.88
CHOMP	540.9 ± 19.9	11.0 ± 14.0	0.99 ± 0.01	0.88 ± 0.09	1.7 ± 0.7
GMP	593.3 ± 20.2	30.8 ± 43.7	0.99 ± 0.01	0.86 ± 0.22	0.03 ± 0.004

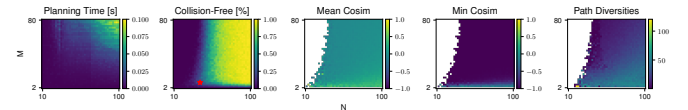


Fig. 4. For each M, N , we set the number of probing $H = 30$ and plan the batch of $B = 200$ paths. The red star denotes the optimal number of layers M_m , corresponding to the minimum requirement of N to discover some solutions.

C. Ablation Study

This section explores various aspects of GTMP by investigating hyperparameter sweeps.

Probabilistic Completeness Ablation. Fig. 4 shows the sweeping statistics of $M \in \{2, \dots, 80\}$, $N \in \{10, \dots, 100\}$ the Intel Lab occupancy map with a chosen start-goal pair to study the probabilistic completeness Theorem 2. Fig. 4 shows experimentally polynomial planning time-complexity after JIT. The CF(%) metric directly reflects the path existence probability Eq. (9). Notice that the minimum layer $M_m = 3$ must be set for collision-free paths in the batch. Interestingly, M_m is also the optimal number of layers to achieve non-zero CF(%) with a minimal point per layer N (red star), which confirms the observation in Section V. Further observations on Min/Mean Cosim also confirm that with less M , the paths are smoother. Finally, higher path diversity is induced by having higher CF(%)

GTMP Hyperparameter Characteristics. In Table III, we ask how many tasks in the Panda MBM dataset can be solved with just one layer since $M = 1$ is a trivial realization of GTMP (i.e., VI is not required at $M = 1$). Solving a task means at least one collision-free path exists in a batch of $B = 50$ paths per problem. We report for GTMP and GTMP-Akima the aggregated planning times of $250 \pm 60\mu s$, $300 \pm 80\mu s$ and Min Cosim of $-0.20 \pm$

0.32, 0.67 ± 0.14 , respectively. Although not comparable to CHOMP and GPMP in smoothness, one-layer GTMP solves many tasks due to maximum exploration characteristics, compared to local methods such as trajectory optimizers requiring gradients.

VII. DISCUSSION & CONCLUSIONS

GTMP offers several advantages algorithmically, as it is *vectorizable* over a large number of planning instances, it does not require *joint-limit enforcement* (i.e., sampling points in the limits), *gradients* or *simplification routines*. On the practical side, GTMP is *easy to implement* (i.e., only tensor manipulation), *easy to tune* (i.e., hyperparameter set $(M, N, H, \gamma = 0.99)$), and *easy to incorporate* motion planning objectives in Eq. (16).

However, we do not argue for replacing classical sampling-based algorithms such as RRT with GTMP; rather, using it as a complementary tool. GTMP excels as a generator of diverse, globally optimal trajectories for dataset creation, whereas RRT variants focus on rapid single-path execution.

GTMP addresses global exploration challenges but comes with memory requirements, especially for GPU acceleration. In contrast, local methods such as CHOMP or GPMP leverage gradient-based, more memory-efficient trajectory optimization. GTMP-Akima, for instance, avoids the need for gradients while delivering smooth velocity trajectories by a *spline discretization structure*, making it a viable initialization for methods like GPMP, potentially combining the strengths of both approaches.

Variants of GTMP emphasize maximum exploration while maintaining smooth trajectory structures. Exploring further smooth discretization structures for higher-order planning is exciting, as the current Akima discretization structure only provides a C^1 spline grid. Furthermore, we are eager to adopt the efficient collision-checking of VAMP [23] for GTMP, when the VAMP batching configuration collision-checking becomes available. Lastly, GTMP suggests the direction of probabilistically-complete batch planners, serving as a differentiable global planner or a competent oracle for learning.

APPENDIX

The Akima spline [20], [35] is a piecewise cubic interpolation method that exhibits C^1 smoothness by using local points to construct the spline, avoiding oscillations or overshooting in other interpolation methods, such as cubic splines or B-splines.

Definition 4 (Akima Spline). *Given a point set $\{\mathbf{q}_i | \mathbf{q} \in \mathcal{C}\}_{i=1}^P$, the Akima spline constructs a piecewise cubic polynomial $f(t)$ for each interval $[t_i, t_{i+1}]$*

$$f_i(t) = \mathbf{d}_i(t - t_i)^3 + \mathbf{c}_i(t - t_i)^2 + \mathbf{b}_i(t - t_i) + \mathbf{a}_i, \quad (11)$$

TABLE III

SUCCESS RATE COMPARISON OVER MOTION BENCH MAKER DATASET

Algorithms	bookshelf_small	bookshelf_tall	bookshelf_thin	box	cage	table_pick	table_under_pick
GTMP (N=200, M=1)	100	100	100	100	57	62	100
GTMP-Akima (N=200, M=1)	85	94	78	95	83	91	29
GTMP (N=30, M=2)	100	100	100	100	26	100	100
GTMP-Akima (N=30, M=2)	91	98	86	96	67	95	67
CHOMP	83	96	98	76	0	93	22
GPMP	56	72	47	16	51	51	0

where the coefficients $\mathbf{a}_i, \mathbf{b}_i, \mathbf{c}_i, \mathbf{d}_i \in \mathcal{C}$ are determined from the conditions of smoothness and interpolation. Let $\mathbf{m}_i = (\mathbf{q}_{i+1} - \mathbf{q}_i)/(t_{i+1} - t_i)$ at t_i , the spline slope is computed from m_{i-1}, m_{i+1}

$$\mathbf{s}_i = \frac{|\mathbf{m}_{i+1} - \mathbf{m}_i| \mathbf{m}_{i-1} + |\mathbf{m}_{i-1} - \mathbf{m}_{i-2}| \mathbf{m}_i}{|\mathbf{m}_{i+1} - \mathbf{m}_i| + |\mathbf{m}_{i-1} - \mathbf{m}_{i-2}|}. \quad (12)$$

The spline slopes for the first two points at both ends are $\mathbf{s}_1 = \mathbf{m}_1, \mathbf{s}_2 = (\mathbf{m}_1 + \mathbf{m}_2)/2, \mathbf{s}_{P-1} = (\mathbf{m}_{P-1} + \mathbf{m}_{P-2})/2, \mathbf{s}_P = \mathbf{m}_{P-1}$. Then, the polynomial coefficients are uniquely defined

$$\begin{aligned} \mathbf{a}_i &= \mathbf{q}_i, & \mathbf{b}_i &= \mathbf{s}_i, \\ \mathbf{c}_i &= (3\mathbf{m}_i - 2\mathbf{s}_i - \mathbf{s}_{i+1})/(t_{i+1} - t_i), \\ \mathbf{d}_i &= (\mathbf{s}_i + \mathbf{s}_{i+1} - 2\mathbf{m}_i)/(t_{i+1} - t_i)^2. \end{aligned} \quad (13)$$

The Akima spline slope is determined by the local behavior of the data points, preventing oscillations that can occur when using global information. Interpolating with Akima spline does not require solving large systems of linear equations, making it computationally efficient as an ideal extension to Definition 2 to a *spline discretization structure*.

Definition 5 (Akima Spline Graph). *Given a geometric graph $G = (\mathcal{V}, \mathcal{E})$ (cf. Definition 2), the Akima Spline graph G_A has the edge set \mathcal{E} geometrically augmented by cubic polynomials. In particular, consider an edge $(\mathbf{q}_{m,i}, \mathbf{q}_{m+1,j}) \in \mathcal{E}$ with i, j are respective indices of points at layers $\mathcal{L}_m, \mathcal{L}_{m+1}$, the spline slope is defined with $\mathbf{m}_{m,i,j} = (\mathbf{q}_{m+1,j} - \mathbf{q}_{m,i})/(t_{i+1} - t_i)$ as Modified Akima interpolation [20]*

$$\begin{aligned} s_{m,i,j} &= \frac{w_{m,i,j} m_{m-1,i,j} + w_{m-1,i,j} m_{m,i,j}}{w_{m,i,j} + w_{m-1,i,j}} \\ w_{m,i,j} &= \left| \frac{1}{N^2} \sum_{i,j} m_{m+1,i,j} - m_{m,i,j} \right| + \left| \frac{1}{2} \left| \frac{1}{N^2} \sum_{i,j} m_{m+1,i,j} + m_{m,i,j} \right| \right| \\ w_{m-1,i,j} &= \left| m_{m-1,i,j} - \frac{1}{N^2} \sum_{i,j} m_{m-2,i,j} \right| + \left| \frac{1}{2} \left| m_{m-1,i,j} + \frac{1}{N^2} \sum_{i,j} m_{m-2,i,j} \right| \right|. \end{aligned} \quad (14)$$

Then, the augmented cubic polynomial $f_{i,j}(t), t \in [t_m, t_{m+1}]$ is computed following Eq. (13)

$$\begin{aligned} \mathbf{s}_m &= \frac{1}{N^2} \sum_{i,j} s_{m,i,j}, & \mathbf{a}_{m,i,j} &= \mathbf{q}_{m,i}, & \mathbf{b}_{m,i,j} &= \mathbf{s}_m, \\ \mathbf{c}_{m,i,j} &= (3\mathbf{m}_{m,i,j} - 2\mathbf{s}_m - \mathbf{s}_{m+1})/(t_{m+1} - t_m), \\ \mathbf{d}_{m,i,j} &= (\mathbf{s}_m + \mathbf{s}_{m+1} - 2\mathbf{m}_{m,i,j})/(t_{m+1} - t_m)^2. \end{aligned} \quad (15)$$

The original Akima interpolation [35] computes equal weight to the points on both sides, evenly dividing an undulation. When two flat regions with different slopes meet, this modified Akima interpolation [20] gives more weight to the side where the slope is closer to zero, thus giving priority to the side that is closer to horizontal, which avoids overshoot. Notice that after pre-computing $\mathbf{m}_{m,i,j}$ for every edge in G_A , every polynomial segment Eq. (15) can be computed in batch for G_A . Furthermore, given a batch of graphs G_A , adding a batch dimension for these equations is straightforward. The transition cost is then defined

$$c(\mathbf{q}, \mathbf{q}') = \int_a^b (c_{\text{coll}}(f(t)) + 1) \|f'(t)\| dt, \quad (16)$$

where $f(t)$ is the cubic polynomial representing the edge $(\mathbf{q}, \mathbf{q}') \in G_A$.

Remark 1. *With some algebra derivations, one can verify the cubic polynomial $f_{i,j}(t)$, $t \in [t_m, t_{m+1}]$ representing any edge $(\mathbf{q}_{m,i}, \mathbf{q}_{m+1,j}) \in G_A$ satisfying four conditions of continuity*

$$\begin{aligned} f_{i,j}(t_m) &= \mathbf{q}_{m,i}, f_{i,j}(t_{m+1}) = \mathbf{q}_{m+1,j}, \\ f'_{i,j}(t_m) &= \mathbf{s}_m, f'_{i,j}(t_{m+1}) = \mathbf{s}_{m+1}, \end{aligned} \quad (17)$$

for any $m \in \{0, \dots, M+1\}$, $i, j \in \{1, \dots, N\}$. Hence, any path $f \in G_A$ is an Akima spline.

The Akima spline provides C^1 -continuity for first-order planning; however, the second derivative is not necessarily continuous. Note that Theorem 2 does not necessarily hold for Akima Spline Graph G_A and is left for future work.

ACKNOWLEDGMENT

An T. Le was funded by the German Research Foundation project METRIC4IMITATION (PE 2315/11-1). Kay Hansel received funding from CHIRON by DFG (PE 2315/8-1), the European Union's Horizon Europe program, under Grant Agreement No. 101135959 (project ARISE).

REFERENCES

- [1] L. E. Kavraki, P. Svestka, J.-C. Latombe, and M. H. Overmars, "Probabilistic roadmaps for path planning in high-dimensional configuration spaces," *IEEE Transactions on Robotics and Automation*, 1996.
- [2] J. J. Kuffner and S. M. LaValle, "Rrt-connect: An efficient approach to single-query path planning," in *IEEE ICRA*, 2000.
- [3] J.-C. Latombe, *Robot motion planning*. Springer Science & Business Media, 2012, vol. 124.
- [4] J. Carvalho, A. T. Le, M. Baierl, D. Koert, and J. Peters, "Motion planning diffusion: Learning and planning of robot motions with diffusion models," in *IEEE/RSJ IROS*, 2023.
- [5] J. Wang, T. Zhang, N. Ma, Z. Li, H. Ma, F. Meng, and M. Q.-H. Meng, "A survey of learning-based robot motion planning," *IET Cyber-Systems and Robotics*, vol. 3, no. 4, pp. 302–314, 2021.
- [6] M. Reuss, M. Li, X. Jia, and R. Lioutikov, "Goal conditioned imitation learning using score-based diffusion policies," in *R:SS*, 2023.
- [7] A. T. Le, G. Chalvatzaki, A. Biess, and J. R. Peters, "Accelerating motion planning via optimal transport," *NeurIPS*, vol. 36, 2024.
- [8] M. Mukadam, J. Dong, X. Yan, F. Dellaert, and B. Boots, "Continuous-time gaussian process motion planning via probabilistic inference," *IJRR*, 2018.
- [9] T. Osa, "Multimodal trajectory optimization for motion planning," *IJRR*, 2020.
- [10] M. Bhardwaj, B. Sundaralingam, A. Mousavian, N. D. Ratliff, D. Fox, F. Ramos, and B. Boots, "Storm: An integrated framework for fast joint-space model-predictive control for reactive manipulation," in *CoRL*. PMLR, 2022.
- [11] B. Sundaralingam, S. K. S. Hari, A. Fishman, C. Garrett, K. Van Wyk, V. Blukis, A. Millane, H. Oleynikova, A. Handa, F. Ramos, *et al.*, "Curobo: Parallelized collision-free robot motion generation," in *IEEE ICRA*, 2023.
- [12] J. Pan and D. Manocha, "Gpu-based parallel collision detection for fast motion planning," *IJRR*, 2012.
- [13] J. Bialkowski, S. Karaman, and E. Frazzoli, "Massively parallelizing the rrt and the rrt*," in *IEEE/RSJ IROS*, 2011.
- [14] J. Blankenburg, R. Kelley, D. Feil-Seifer, R. Wu, L. Barford, and F. C. Harris, "Towards gpu-accelerated prm for autonomous navigation," in *ITNG*. Springer, 2020.
- [15] S. A. Jacobs, K. Manavi, J. Burgos, J. Denny, S. Thomas, and N. M. Amato, "A scalable method for parallelizing sampling-based motion planning algorithms," in *IEEE ICRA*, 2012.
- [16] P. E. Hart, N. J. Nilsson, and B. Raphael, "A formal basis for the heuristic determination of minimum cost paths," *IEEE Transactions on Systems Science and Cybernetics*, vol. 4, no. 2, pp. 100–107, 1968.

- [17] S. J. Russell and P. Norvig, *Artificial intelligence: a modern approach*. Pearson, 2016.
- [18] J. Bradbury *et al.*, "JAX: composable transformations of Python+NumPy programs," 2018. [Online]. Available: <http://github.com/google/jax>
- [19] I. A. Sucan, M. Moll, and L. E. Kavraki, "The open motion planning library," *IEEE Robotics & Automation Magazine*, 2012.
- [20] H. Akima, "A method of bivariate interpolation and smooth surface fitting based on local procedures," *Communications of the ACM*, vol. 17, no. 1, pp. 18–20, 1974.
- [21] N. M. Amato and L. K. Dale, "Probabilistic roadmap methods are embarrassingly parallel," in *IEEE ICRA*, 1999.
- [22] E. Plaku, K. E. Bekris, B. Y. Chen, A. M. Ladd, and L. E. Kavraki, "Sampling-based roadmap of trees for parallel motion planning," *IEEE Transactions on Robotics*, vol. 21, no. 4, pp. 597–608, 2005.
- [23] W. Thomason, Z. Kingston, and L. E. Kavraki, "Motions in microseconds via vectorized sampling-based planning," in *IEEE ICRA*, 2024.
- [24] J. D. Gammell, T. D. Barfoot, and S. S. Srinivasa, "Batch informed trees (bit*): Informed asymptotically optimal anytime search," *IJRR*, 2020.
- [25] L. Janson, E. Schmerling, A. Clark, and M. Pavone, "Fast marching tree: A fast marching sampling-based method for optimal motion planning in many dimensions," *IJRR*, 2015.
- [26] M. P. Strub and J. D. Gammell, "Adaptively informed trees (ait*): Fast asymptotically optimal path planning through adaptive heuristics," in *IEEE ICRA*, 2020.
- [27] J. Wang, W. Chi, C. Li, C. Wang, and M. Q.-H. Meng, "Neural rrt*: Learning-based optimal path planning," *IEEE Transactions on Automation Science and Engineering*, 2020.
- [28] C. Yu and S. Gao, "Reducing collision checking for sampling-based motion planning using graph neural networks," *Advances in Neural Information Processing Systems*, vol. 34, pp. 4274–4289, 2021.
- [29] B. Ichter, J. Harrison, and M. Pavone, "Learning sampling distributions for robot motion planning," in *IEEE ICRA*, 2018.
- [30] A. Orthey, C. Chamzas, and L. E. Kavraki, "Sampling-based motion planning: A comparative review," *Annual Review of Control, Robotics, and Autonomous Systems*, vol. 7, 2023.
- [31] V. K. Adajania, A. Sharma, A. Gupta, H. Masnavi, K. M. Krishna, and A. K. Singh, "Multi-modal model predictive control through batch non-holonomic trajectory optimization: Application to highway driving," *IEEE RA-L*, 2022.
- [32] A. Lambert, A. Fishman, D. Fox, B. Boots, and F. Ramos, "Stein variational model predictive control," *arXiv:2011.07641*, 2020.
- [33] J. Urain, A. T. Le, A. Lambert, G. Chalvatzaki, B. Boots, and J. Peters, "Learning implicit priors for motion optimization," in *IEEE/RSJ IROS*, 2022.
- [34] S. M. LaValle, *Planning algorithms*. Cambridge university press, 2006.
- [35] H. Akima, "A new method of interpolation and smooth curve fitting based on local procedures," *Journal of the ACM (JACM)*, vol. 17, no. 4, pp. 589–602, 1970.
- [36] M. L. Puterman, *Markov decision processes: discrete stochastic dynamic programming*. John Wiley & Sons, 2014.
- [37] D. Bertsekas, *Dynamic programming and optimal control: Volume I*. Athena scientific, 2012, vol. 4.
- [38] D. Bertsekas and J. Tsitsiklis, *Parallel and distributed computation: numerical methods*. Athena Scientific, 2015.
- [39] M. L. Littman, T. L. Dean, and L. P. Kaelbling, "On the complexity of solving markov decision problems," *arXiv preprint arXiv:1302.4971*, 2013.
- [40] E. Coumans and Y. Bai, "Pybullet, a python module for physics simulation for games, robotics and machine learning," <http://pybullet.org>, 2016–2019.
- [41] M. Zucker *et al.*, "Chomp: Covariant hamiltonian optimization for motion planning," *IJRR*, 2013.
- [42] M. Cuturi, "Sinkhorn distances: Lightspeed computation of optimal transport," *NeurIPS*, 2013.
- [43] I. A. Şucan and L. E. Kavraki, "Kinodynamic motion planning by interior-exterior cell exploration," in *WAFR*. Springer, 2009.
- [44] A. Howard, N. Roy, C. Stachniss, G. Grisetti, D. Haehnel, H. Andreasson, P. Larsson, T. Duckett, and P. Beeson, "The robotics data set repository (radish)," 2003. [Online]. Available: <http://radish.sourceforge.net/>
- [45] C. Chamzas, C. Quintero-Pena, Z. Kingston, A. Orthey, D. Rakita, M. Gleicher, M. Toussaint, and L. E. Kavraki, "Motionbenchmarker: A tool to generate and benchmark motion planning datasets," *IEEE RA-L*, 2021.